ACS chemical biology

pubs.acs.org/acschemicalbiology

Articles

Unraveling Molecular Recognition of Glycan Ligands by Siglec-9 via NMR Spectroscopy and Molecular Dynamics Modeling

Unai Atxabal, Corwin Nycholat, Johannes M. Pröpster, Andrea Fernández, Iker Oyenarte, Maria Pia Lenza, Antonio Franconetti, Cátia O. Soares, Helena Coelho, Filipa Marcelo, Mario Schubert, James C. Paulson, Jesús Jiménez-Barbero,* and June Ereño-Orbea*

Cite This: *ACS Chem. Biol.* 2024, 19, 483−496

Read Online

ACCESS | Metrics & More | Article Recommendations | Supporting Information

ABSTRACT: Human sialic-acid-binding immunoglobulin-like lectin-9 (Siglec-9) is a glycoimmune checkpoint receptor expressed on several immune cells. Binding of Siglec-9 to sialic acid containing glycans (sialoglycans) is well documented to modulate its functions as an inhibitory receptor. Here, we first assigned the amino acid backbone of the Siglec-9 V-set domain (Siglec-9_{d1}), using well-established triple resonance three-dimensional nuclear magnetic resonance (NMR) methods. Then, we combined solution NMR and molecular dynamic simulation methods to decipher the molecular details of the interaction of Siglec-9 with the natural ligands α2,3 and α2,6 sialyl lactosamines (SLN), sialyl Lewis X (sLeX), and 6-O sulfated sLeX and with two synthetically modified sialoglycans that bind with high affinity. As expected, Neu5Ac is accommodated between the F and G β-strands at the canonical sialic acid binding site. Addition of a heteroaromatic scaffold 9*N*-5-(2-methylthiazol-4-yl)thiophene sulfonamide (MTTS) at the C9 position of Neu5Ac generates new interactions with the hydrophobic residues located at the G−G′ loop and the N-terminal region of Siglec-9. Similarly, the addition of the aromatic substituent (5-*N*-(1-benzhydryl-1*H*-1,2,3-triazol-4-yl)methyl (BTC)) at the C5 position of Neu5Ac stabilizes the conformation of the long and flexible B′−C loop present in Siglec-9. These results expose the underlying mechanism responsible for the enhanced affinity and specificity for Siglec-9 for these two modified sialoglycans and sheds light on the rational design of the next generation of modified sialoglycans targeting Siglec-9.

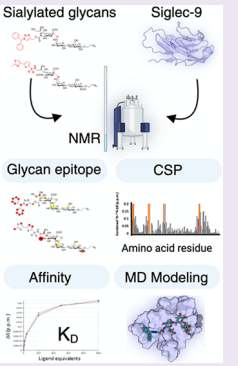

INTRODUCTION

The sialic-acid-binding immunoglobulin-type lectin (Siglec)-9 is an immune checkpoint receptor that is widely expressed on several types of immune cells, including monocytes, neutrophils, dendritic cells, macrophages, as well as certain subsets of natural killer (NK) and T cells.[1] Siglec-9 binds to various sialic acid containing glycans (sialoglycans) through its extracellular domain (ECD), thereby triggering inhibitory responses via the immunoreceptor tyrosine-based inhibitory motifs (ITIMs) and ITIM-like motifs located at the intracellular tail.[2,3] Siglec-9 is of particular interest in the context of tumor immunotherapy, since it has been recognized that various human cancers express sialoglycans recognized by this receptor.[4] Diverse evidence shows that engagement of Siglec-9 expressed on immune cells by sialoglycan-decorated cancer cells leads to an attenuation of both myeloid and lymphoid antitumor responses.[5] In this respect, Siglec-9 offers therapeutic opportunities that are differentiated from and complementary to the classic immune-checkpoint receptor blockade (e.g., PD-1/PD.1L).[6−10] Currently anti-Siglec-9 antibodies that can block binding to sialoglycans are under preclinical studies and have been shown to restore the immune response within the tumor microenvironment.[11,12]

Chemically modified glycan and glycomimetic ligands constitute a promising class of molecules to target Siglecs.[13] For being able to compete with the natural ligands, these synthetic glycans must present strong affinities for overcoming the avidity of the densely presented natural glycan ligands, including endogenous *cis* glycans that may mask the binding groove of Siglecs.[13] The use of liposomes or nanoparticles decorated with modified glycans with enhanced affinities has shown promising results for modulating the Siglec−sialic acid axis.[14,15] Such is the case of the high affinity ^{NSA}Neu5Ac analogue for Siglec-8, which was found to be a high affinity ligand for Siglec-8. Indeed, antigenic liposomes displaying an antigen and the ^{NSA}Neu5Ac mimetic were able to suppress the activation of mast cells sensitized with an antiallergen IgE.[16] We have also described decoration of the Neu5Ac moiety with a triazole linked benzhydryl substituent at the C5 position in Neu5Ac ((5-*N*-[(1-benzhydryl-1*H*-1,2,3-triazol-4-yl)methyl carbamate]-Neu5Acα(2−6)Galβ(1−4)GlcNAc), ^{BTC}Neu5Ac; Figure 1) that provides a selective ligand for Siglec-9.[17] It was found that ^{BTC}Neu5Ac attached to liposomal nanoparticles

Received: October 30, 2023
Revised: January 9, 2024
Accepted: January 16, 2024
Published: February 7, 2024

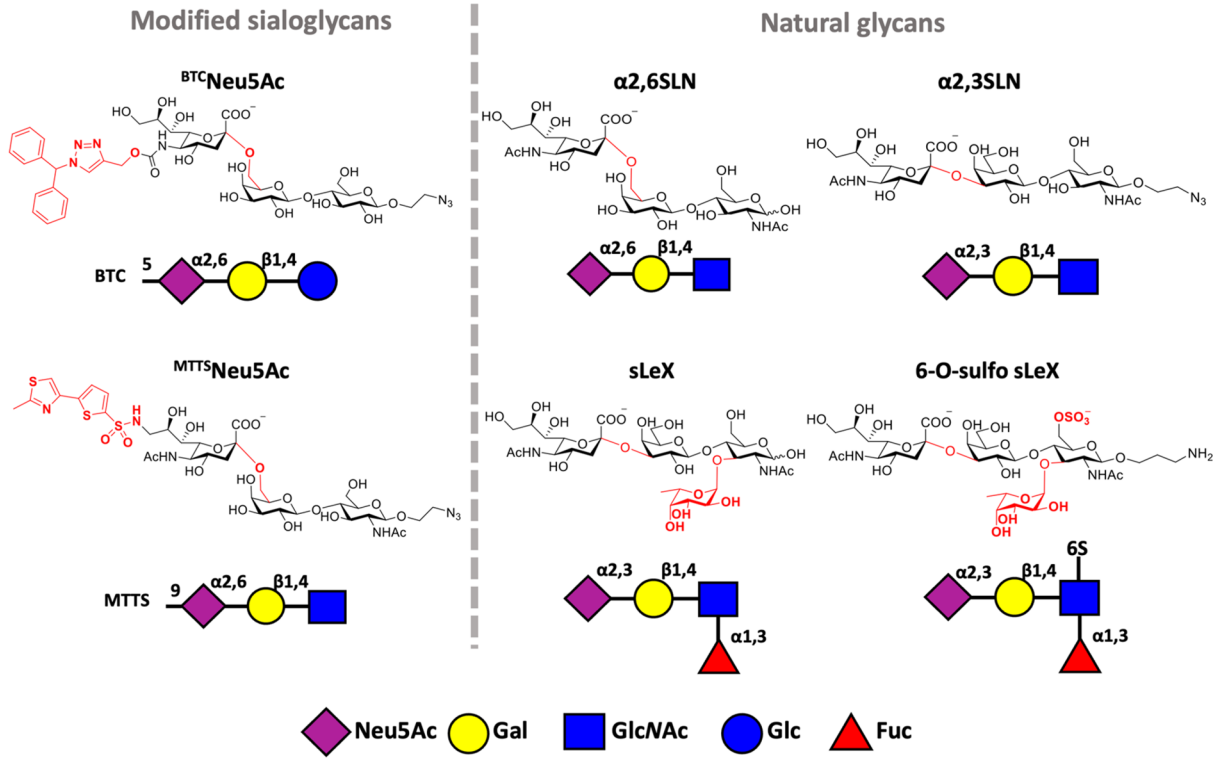

Figure 1. Studied natural and synthetic sialoglycans. The chemical structures of the sialoglycans studied here are shown. Monossacharides are also represented with the symbol nomenclature for glycans (SNFG).

effectively binds to Siglec-9 expressed on the surface of Chinese hamster ovary (CHO) cells even in the presence of *cis* ligands, which triggers a rapid endocytic response.[17] Moreover, ^{BTC}Neu5Ac attached to a lipopeptide efficiently blocks ligand-binding to Siglec-9 expressed in neutrophils, inhibiting proinflammatory signals and inflammation induced by COVID-19.[18] Lipid-linked glycopeptides decorated with ^{BTC}Neu5Ac can also be inserted into the cell membrane of macrophages and outcompete *cis* glycan binders of Siglec-9, suppressing macrophage activity.[19]

Given the array of applications that ^{BTC}Neu5Ac displays, we herein disclose the structural and conformational determinants of the interaction of ^{BTC}Neu5Ac with Siglec-9, using nuclear magnetic resonance (NMR) methods, from both the ligands and receptors perspective. Additionally, following the analogous approach, we have analyzed the interaction of the 9*N*-[5-(2-methylthiazol-4-yl)thiophene sulfonamide]-Neu5Acα(2−6)Galβ(1−4)GlcNAc analogue (^{MTTS}Neu5Ac), which is modified at the C9 of the sialic acid[15] (Figure 1). In the absence of any three-dimensional structure for the ECD of Siglec-9, we have assigned the amino acid backbone in the NMR spectrum of the variable (V)-immunoglobulin (Ig)-set domain of Siglec-9 (Siglec-9_{d1}), which harbors the carbohydrate recognition domain.[20,21] The NMR assignment of the protein backbone has allowed us to track the changes in the V-set domain upon ligand binding by using the chemical shift perturbation (CSP)-NMR methodology. The affinities for Siglec-9 of ^{MTTC}Neu5Ac and ^{BTC}Neu5Ac are in the low micromolar range, as calculated from the experimentally derived CSPs and by isothermal titration calorimetry (ITC). Interestingly, ^{MTTC}Neu5Ac (K_D = 9.6 ± 0.8 μM determined by ITC) has shown approximately 2-fold higher affinity toward Siglec-9 than ^{BTC}Neu5Ac (K_D = 19.5 ± 1.3). Both exhibit >20-fold higher affinity for Siglec-9 than the glycan with unsubstituted Neu5Ac.[22] For interpretation of the results, docking and molecular dynamics (MD) calculations have also been performed. Based on a 76% amino acid sequence similarity, the three-dimensional (3D) model of the Siglec-9 V-set domain was generated from the crystal structure of Siglec-7.[23] Overall, Siglec-9 possesses a long and flexible B−C′ loop, composed of three extra aromatic amino acids in comparison with Siglec-7. This feature makes the accommodation of Neu5Ac containing aromatic moieties at position C5 suitable.

RESULTS

NMR Assignment of the Backbone ^{1}H and ^{15}N Nuclei of the Siglec-9 V-Ig Domain. The resonances of the backbone ^{1}H, ^{15}N, and ^{13}C nuclei of the Siglec-9 V-set domain (Siglec-9_{d1}) were assigned using recombinant isotopically labeled protein expressed in the folded form[24] together with well-established triple resonance three-dimensional NMR methods (Figure S1). During the assignment of Siglec-9_{d1}, a peak doubling was unexpectedly observed for several amino acid residues. As the largest chemical shift deviations between the two sets of signal occur in the B′−C loop and four proline residues (P40, P46, P53, and P55) are located in this loop (Figure 2A), the signal doubling was suspected to be caused by a Pro cis/trans isomerization event.[25] The ^{13}C chemical shifts of these prolines indeed confirmed that the signal doubling was caused by the P53 residue (observed δ cis C_β = 33.8 ppm, δ trans C_β = 31.4 ppm obtained from a CBCA(CO)NH), which are typical values for *cis*- and *trans*-Pro peptide bonds (average δ cis Cβ = 34.2 ppm, δ trans Cβ = 31.8 ppm).[23,25] It was concluded that 71% of the species corresponded to *cis* P53 while 29% corresponded to the *trans* form. The use of a P53S mutant allowed assignment of the doubled peaks (Figure 2B),

https://doi.org/10.1021/acschembio.3c00664
ACS Chem. Biol. 2024, 19, 483−496

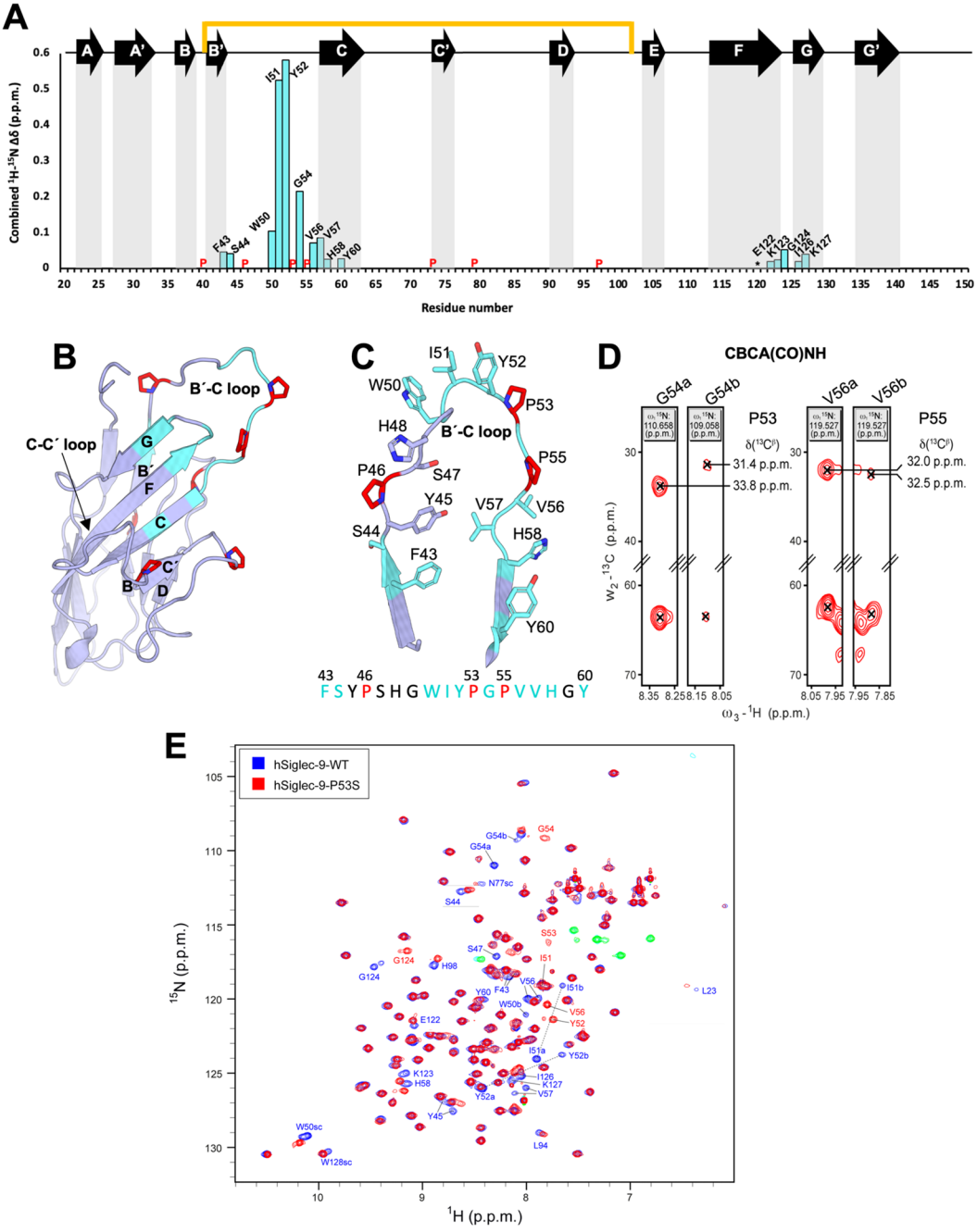

Figure 2. Amino acid sequence assignment of the Siglec-9_{d1} protein backbone and observed peak doubling. (A) Combined ^{1}H and ^{15}N chemical shift differences between the two sets of observed amide backbone resonances plotted over the residue number. Unassigned backbone residues are indicated by asterisks and proline residues with P. (B) Homology model of Siglec-9_{d1} (residues 18−142) generated by RoseTTA Fold[32,56] depicted in cartoon representation. Conserved β-strands are labeled with letters. Residues with peak doubling are colored in cyan, while prolines shown as sticks are colored in red. (C) Close-up view of the B′−C loop. (D) ^{13}C axis of a 3D CBCA(CO)NH spectrum of Siglec-9_{d1} of both signals sets for residues Gly54 and Val57 showing the different Cβ chemical shifts of Pro53 and Pro55, respectively. The major form is indicated by set a, the minor form by set b. (E) Comparison of the ^{1}H−^{15}N HSQC spectra of Siglec-9_{d1} and a P53S point mutant protein that does not display the *cis*-Pro peptide bond.

and only one set of signals corresponding to the trans conformation was left. Some residues, especially those adjacent to P53 within the B′−C loop but also others relatively distant in the primary sequence, presented peak doubling (Figure 2B). The relative intensities showed that the equilibrium is shifted toward a major *cis* conformer.

The Epitopes of the Glycans Recognized by Siglec-9. Saturation transfer difference (STD)-NMR experiments were carried out with each of the ^{BTC}Neu5Ac and ^{MTTS}Neu5Ac and the full extracellular domain (EDC) of Siglec-9 containing the V-set and two C2-set Ig-like domains (Siglec-9_{d1-d3}) to map the ligand binding epitopes. The success of STD-NMR and trNOESY experiments depends, among other factors, on the rotational correlation time of the receptor, which is dependent on its molecular size. Thus, the complete ECD instead of the simple V-Ig domain was employed to carry out these experiments to improve the signal-to-noise ratio in the STD-NMR and trNOESY experiments. For comparison purposes,

https://doi.org/10.1021/acschembio.3c00664
ACS Chem. Biol. 2024, 19, 483−496

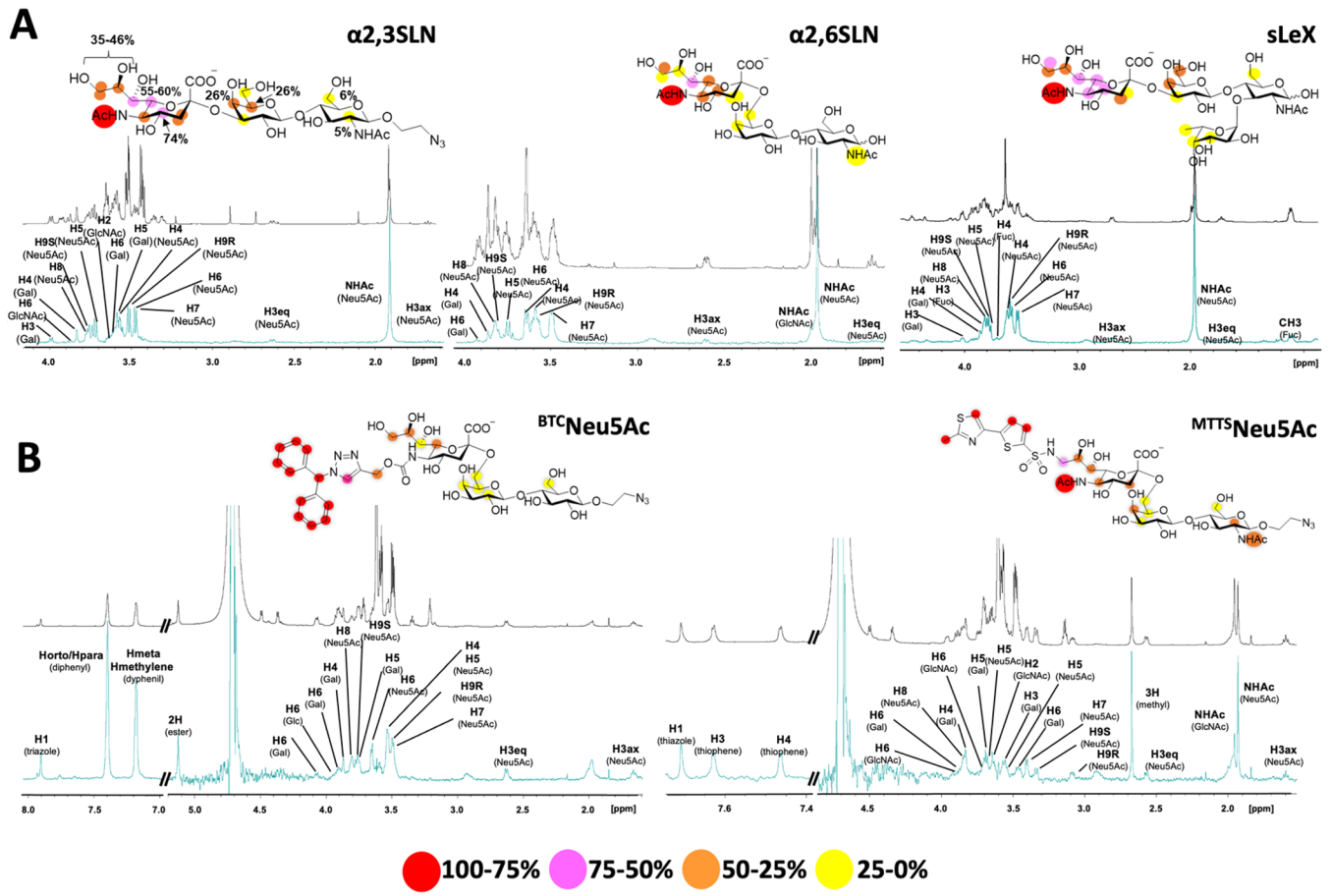

Figure 3. STD-NMR epitope mapping of α2,3SLN, α2,6SLN, sLeX, ^{BTC}Neu5Ac, and ^{MTTS}Neu5Ac sialoglycans. (A) Reference off-resonance spectrum (black) and STD-NMR spectra with 50× amplification (cyan) of the Siglec-$9_{d1\text{-}d3}$ and α2,3SLN, α2,6SLN, or sLeX in molar ratio of 1:40 (Siglec-9: ligand). STD-based epitope mapping for α2,3SLN, α2,6SLN, or sLeX are also indicated. (B, left) Reference off-resonance spectrum (black) and STD-NMR spectra (50×; cyan) of the Siglec-$9_{d1\text{-}d3}$ and ^{BTC}Neu5Ac in molar ratio of 1:40 (Siglec-9/ligand). (Right) STD-NMR spectra (25×; cyan) of Siglec-9 and ^{MTTS}Neu5Ac in in molar ratio of 1:40 (Siglec-9: ligand). STD-based epitope mapping in ^{BTC}Neu5Ac and ^{MTTS}Neu5Ac are indicated. The relative STD response is color-coded according to the legend.

the binding of the same Siglec-9 construct to the natural α2,3SLN (Neu5Acα(2-3)Galβ(1-4)GlcNAc(β1-OEtN_3), α2,6SLN (Neu5Acα(2-6)Galβ(1-4)GlcNAc), sLeX (Neu5Ac-(α2-3)Gal(β1-4)[Fuc(1-3)]GlcNAc), and 6-*O*-sulfated sLeX (Neu5Acα(2-6)Galβ(1-4)6-*O*-sulfoGlcNAc(β1-OPrNH_2) ligands were assessed in separate experiments using the same methodology. As a control experiment, the binding of sLeX to mVENUS did not produce any STD NMR signals (Figure S2). Furthermore, the comparison of the binding epitope obtained by employing the full ECD domain as a receptor yielded results consistent with those obtained when the single V-Ig domain was used (Figure S2), confirming that the binding specificity of the tested sialoside ligands corresponds to the V-Ig domain. The analysis of the data (Tables S1−S5 and Figure S3) showed that, in all cases, the sialic acid moiety gives the highest STD intensities among the natural ligands, with the largest relative STD intensity for the *N*-acetyl group (Figure 3A). Nevertheless, H6, H7, and H9S of the Neu5Ac glycerol moiety also displayed high intensities, indicating the importance of the lateral chain for binding.[26] The Gal moiety never displayed significant STD levels, while the Glc*N*Ac moiety ring at the reducing end showed only marginal STD signals.

For ^{BTC}Neu5Ac, the benzhydryl scaffold showed the highest STD intensities, followed by proton at the triazole ring (Figure 3B). The methylene moiety did not show significant saturation levels, while the sialic acid moiety also displayed large intensities. For ^{MTTS}Neu5Ac, all protons at the 5-(2-methylthiazol-4-yl)thiophene presented very similar and high STD intensities, even larger than those of the *N*-acetyl group of Neu5Ac (Figure 3B). Interestingly, for both of these Neu5Acα2,6Gal-linked synthetic analogues, very similar STD patterns were found for the Gal and Glc/Glc*N*Ac moieties. In contrast to the observations for the α2,3-linked moieties, the *N*-acetyl group at the GlcNAc moiety of ^{MTTS}Neu5Ac showed significant STD intensity, suggesting that the *N*-acetyl GlcNAc group of this analogue provides some contacts to Siglec-9.

Conformational Analysis of the Glycans Recognized by Siglec-9. The conformational analysis of the α2,3SLN, α2,6SLN, and sLeX ligands in free solution has been extensively analyzed, showing that these trisaccharides display a conformational equilibrium in solution, especially around the Neu5Ac-Gal linkages.[27] Here, we analyzed the conformation of these ligands in the presence of Siglec-$9_{d1\text{-}d3}$ (Figure S4). Only the key H3Gal-H8Neu5Ac NOE remained visible for α2,3SLN and sLeX in the presence of Siglec-9, while the alternative H3Gal-H3Neu5Ac NOE vanished. These experimental data strongly suggest that only the Φ/Ψ −60/0° geometry around the Neu5Acα2,3Gal glycosidic linkage is recognized by Siglec-9. For the Gal(β1,4)GlcNAc glycosidic linkage, the expected H1Gal-H4GlcNAc and H1Gal-H6GlcNAc NOEs were ob-

https://doi.org/10.1021/acschembio.3c00664
ACS Chem. Biol. 2024, 19, 483−496

served, highlighting the recognition of the typical *syn*-exo anomeric conformation around this linkage.[27] Moreover, for sLeX, regarding the Fuc/GlcNAc glycosidic linkage, the presence of the key H5Fuc-H2Gal NOE (Figure S4) indicates that the preferred geometry characterized by the presence of a nonconventional CH−O hydrogen bond between the C5−H5 of Fuc and the O5 of Gal is maintained also in the bound state.[28] Therefore, a conformational selection process is likely to take place around the flexible Neu5Acα2,3Gal linkage, while the geometries for the LacNAc (in α2,3SLN) and LeX core (in sLeX) are kept in their global energetic minima regions.

The highly flexible Neu5Acα2,6Gal linkage in ^{BTC}Neu5Ac and ^{MTTS}Neu5Ac present several interglycosidic NOEs in their Siglec-9_{d1}-bound states between H8Neu5Ac−$H6_{proR}$Gal, $H3_{eq/ax}$Neu5Ac−H4Gal, and $H3_{ax}$Neu5Ac−$H6_{proR}$Gal (Figure S5), suggesting the *tg* ($\Phi/\Psi/\omega$ −60/180°/180°) as the bound major conformer for both molecules (Figure S5). In contrast, the $H3_{eq/ax}$Neu5Ac−$H6_{proR}$Gal and $H3_{ax}$Neu5Ac−$H6_{proR}$Gal cross-peaks are not present in the free form, while the H8Neu5Ac−$H6_{proR}$Gal NOE is significantly less intense (Figure S4), pointing out the occurrence of the conformational selection process that picks the *tg* conformation.[27]

In the presence of Siglec-9_{d1-d3}, the aromatic protons attached to the HN amide at C5 of ^{BTC}Neu5Ac, show a number of intramolecular NOEs to H9, H7, and H6 at the glycerol side chain of Neu5Ac, which were absent in the NOESY recorded for the ligand in the free-state (Figure S5). For the ^{MTTS}Neu5Ac analogue, a H4thiophene−H4thiazole NOE (corresponding to a distance of 2.2 Å) was evidenced in the bound form, which was not observed in the free state (Figure S5). Similarly, additional cross-peaks were detected between the H3thiophene−$H9_{proS/R}$Neu5Ac and H3thiophene−H8Neu5Ac proton pairs, further confirming the selection of Siglec-9 for the *tg* conformer of ^{MTTS}Neu5Ac.

Therefore, similar to that concluded for the natural glycans, conformational selection events are also likely to take place for ^{BTC}Neu5Ac and ^{MTTS}Neu5Ac upon binding to Siglec-9. In principle, this restriction of motion between the free and bound states should be accompanied by an entropy penalty.

Thermodynamics of the Interaction between Siglec-9 and the Glycomimetics ^{BTC}Neu5Ac and ^{MTTS}Neu5Ac. Additional information about the affinity and the thermodynamic profile of the interaction of Siglec-9 with ^{BTC}Neu5Ac and ^{MTTS}Neu5Ac was gained through isothermal titration calorimetry (ITC) experiments. In both cases, the obtained dissociation constants (K_D) were in the low micromolarity range (Figure 4). Interestingly, although both glycomimetics displayed very similar ΔG values, deviating by less than 0.5 kcal/mol, notable differences were found in their entropic and enthalpic contribution profiles. In any case, the typical enthalpy−entropy compensation phenomenon described for glycan−lectin binding[29] was evidenced here (Figure 4). ^{BTC}Neu5Ac presented a slightly lesser entropy penalty ($-T\Delta S$ = 1.3 kcal/mol) than ^{MTTS}Neu5Ac ($-T\Delta S$ = 3.3 kcal/mol). However, ^{MTTS}Neu5Ac showed a considerably better enthalpy contribution (ΔH = −10.2 kcal/mol) than ^{BTC}Neu5Ac (ΔH = −7.7 kcal/mol).

Mapping the Amino Acid Residues of Siglec-9 Involved in Sialoside Binding. Titration $^{1}H-^{15}N$ HSQC experiments were carried out for ^{BTC}Neu5Ac and ^{MTTS}Neu5Ac interacting with ^{15}N labeled Siglec-9_{d1} (Figure 5). The analysis of the chemical shift perturbations (CSP) in the HSQC cross

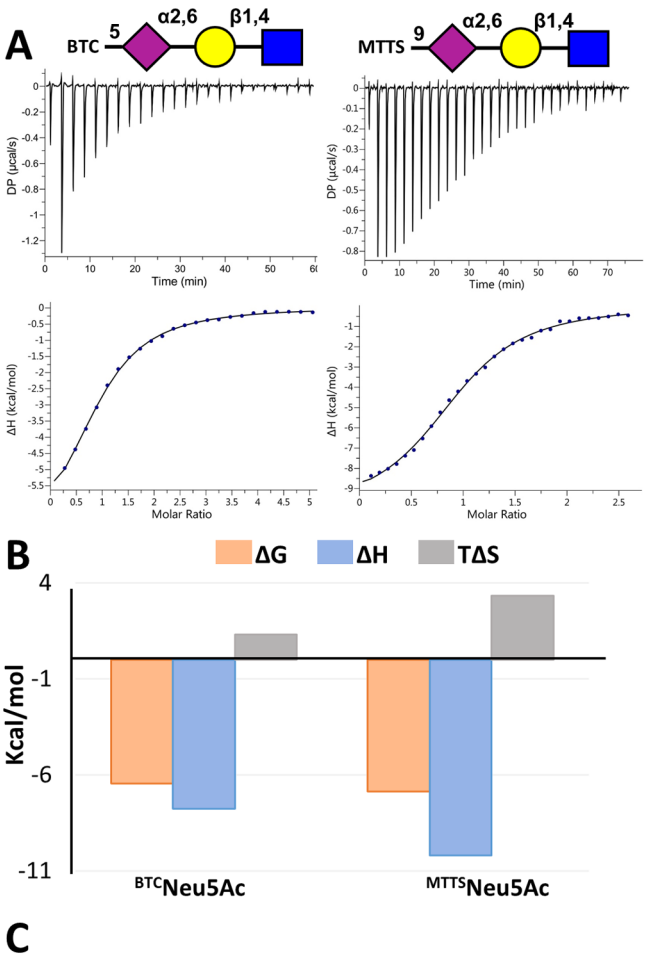

C

Molecule	ΔG (kcal/mol)	ΔH (kcal/mol)	-TΔS (kcal/mol)	K_D (μM)	N (sites)
^{BTC}Neu5Ac	-6.43	-7.76 ± 0.28	1.33	19.5 ± 1.33	0.93 ± 0.02
^{MTTS}Neu5Ac	-6.85	-10.20 ± 0.27	3.34	9.6 ± 0.83	0.97 ± 0.01

Figure 4. Titration with ^{BTC}Neu5Ac or ^{MTSS}Neu5Ac of Siglec-9d1 monitored by ITC. (A) Representative ITC binding isotherms for binding of ^{BTC}Neu5Ac or ^{MTSS}Neu5Ac to Siglec-9_{d1}. (B) The table compares the thermodynamic parameters of binding of ^{BTC}Neu5Ac or ^{MTSS}Neu5Ac to Siglec-9_{d1} as measured by ITC. The values represent the average and standard deviation of triplicates. (C) Table showing the values of the thermodynamic parameters for the interaction of ^{BTC}Neu5Ac and ^{MTSS}Neu5Ac with Siglec-9_{d1} measured by ITC.

peaks of Siglec-9_{d1} allowed deducing of the regions of the V-set domain involved in binding. For comparison, we also analyzed the CSPs on Siglec-9 triggered by binding to α2,3SLN, α2,6SLN, sLeX, and 6-*O*-sulfated sLeX.

The chemical exchange rate of the interaction between Siglec-9_{d1} and the natural sialoglycan ligands α2,3SLN, α2,6SLN, sLeX, and 6-*O*-sulfated sLeX was for most of the $^{1}H-^{15}N$ resonances, within the fast exchange regime in the chemical shift time scale, suggesting that the corresponding dissociation constants are within the high micromolar to millimolar range. As described above, the *cis*−*trans* isomerization equilibrium around the amide linkage of P53 causes signal doubling for some residues (Figure 2). Nevertheless, the fitting of the deviations as a function of ligand concentration showed that there was no significant difference in affinity

https://doi.org/10.1021/acschembio.3c00664
ACS Chem. Biol. 2024, 19, 483−496

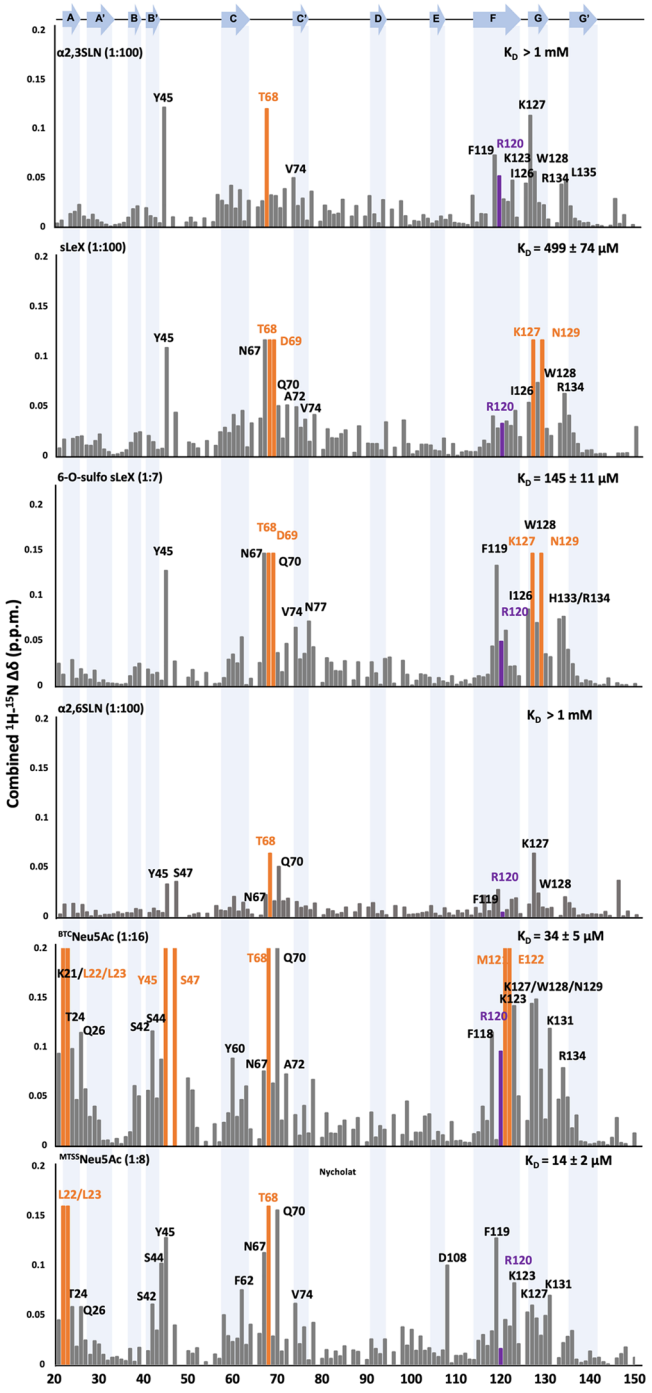

Figure 5. The NMR analysis of the binding of the natural ligands α2,3SLN, α2,6SLN, sLeX, and the modified ^{BTC}Neu5Ac and ^{MTTS}Neu5Ac to Siglec-9 from the lectin's perspective. Combined $^{1}H-^{15}N$ CSP plot ($\Delta\delta$) for ^{15}N-labeled Siglec-9_{d1} residues upon titration with the above presented glycans and glycomimetics, plotted vs the amino acid residues. The secondary structures predicted by the 3D homology model are represented at the top. Residues with significant CSP (2-times higher than the standard deviation) are indicated with gray bars, as well as the estimated dissociation constants. The canonical arginine is indicated with purple bars. The height of the orange bars, which refer to the residues that vanished during the titration, were adjusted to match the level of the most perturbed residue. This adaptation has been implemented to visualize that the disappearance of signals from specific residues is indeed indicative of an interaction between the ligand and the protein at those sites.

between the Pro-*cis* and Pro-*trans* species, at least for the herein tested ligands.

All tested glycans caused CSP of residues within the F and G strands (Figure 5), which correspond to the canonical sialic acid binding site.[13,30] The backbone NH of the canonical R120 at strand F, the residue which is known to be essential for anchoring the Neu5Ac residue via a salt bridge interaction with the C1 carboxylate,[31] was only slightly perturbed in the presence of all the tested sialoglycans. Nevertheless, this observation is not unexpected, since the key interaction involves the positively charged guanidinium of the R120 side chain, remote from the backbone NH. The α2,6SLN ligand induced smaller CSPs compared to α2,3SLN. In this case, minor variations at the C−C′ loop (T68, Q70) and in the F and G strands (K127) were detected. For α2,6SLN, sLeX, and 6-*O*-sulfated sLeX, the most affected residues in Siglec-9 were Y45, F119, R120, I126, K127, and W128, which exhibited CSPs twice higher than the standard deviation (Figure 5). Except for T68, no meaningful CSPs were observed at the C−C′ loop α2,6SLN, the region reported to be responsible for recognizing the glycosidic linkage in other Siglecs.[23] Noticeably for sLeX, large CSPs were observed for N67, T68, D69, and Q70 residues located in the C−C′ loop. Interestingly, the signal for D69 now disappears during the titration (Figure 5), suggesting that the Fuc moiety is located around this protein region. This fact might explain the gain in the estimated binding affinity (K_D 499 ± 74 μM) for sLeX (Figure S6). Simultaneously, at the G strand, significant CSPs were observed for residues I126, K127, N129, H133, and R134. F119 also presents a perturbation, which is located on the F strand. Finally, Y45, despite not being proximate to the binding site but on the B−C′ loop, was also highly perturbed. Cross-peaks of both K127 and N129 vanished during the titration, indicative of a strong interaction with the ligand. The titration with the 6-*O*-sulfo sLeX induced an almost identical CSP pattern in comparison with the nonsulfated sLeX (Figure 5), except for F119, which is located on the F strand (preceding the canonical arginine R120) with its side chain protruding toward the inside of the hydrophobic core. Additionally, the 6-*O*-sulfo sLeX induced higher CSPs than the sLeX with the addition of less equivalents. The measured binding affinity for 6-*O*-sulfo sLeX is 4-fold higher (K_D = 145 ± 10 μM; Figure S7) than that of sLeX.

^{BTC}Neu5Ac and ^{MTTS}Neu5Ac triggered significant CSPs, especially at the C−C′ loop and the F and G strands (Figure 5), much larger than those observed for the natural sialoglycans α2,3SLN, α2,6SLN, sLeX, and 6-*O*-sulfated sLeX, especially in the presence of ^{BTC}Neu5Ac. The amino acid residues within the C−C′ and F−G loops were fairly similar to those observed for the interaction with α2,3SLN, α2,6SLN, sLeX, and 6-*O*-sulfated sLeX. The most perturbed residues within the C−C′ loop were observed for N67, T68, and Q70, whereas in distinction from sLeX and 6-*O*-sulfo sLeX, no perturbation was observed for D69 (Figure 5). Interestingly, for ^{BTC}Neu5Ac, which has additional molecular fragments extended at position NH5 of the sialic acid, the free-bound chemical exchange rate was intermediate in the chemical shift time scale, and a dramatic intensity reduction of several key peaks occurred during the titration. In this case, a K_D of 34 ± 5 μM was estimated from the CSPs (Figure S8), which is in agreement with the values reported by ITC (Figure 4). Indeed, complete saturation of Siglec-9 with ^{BTC}Neu5Ac was achieved by adding 16 equiv of ligand. Substantial CSPs

https://doi.org/10.1021/acschembio.3c00664
ACS Chem. Biol. 2024, 19, 483−496

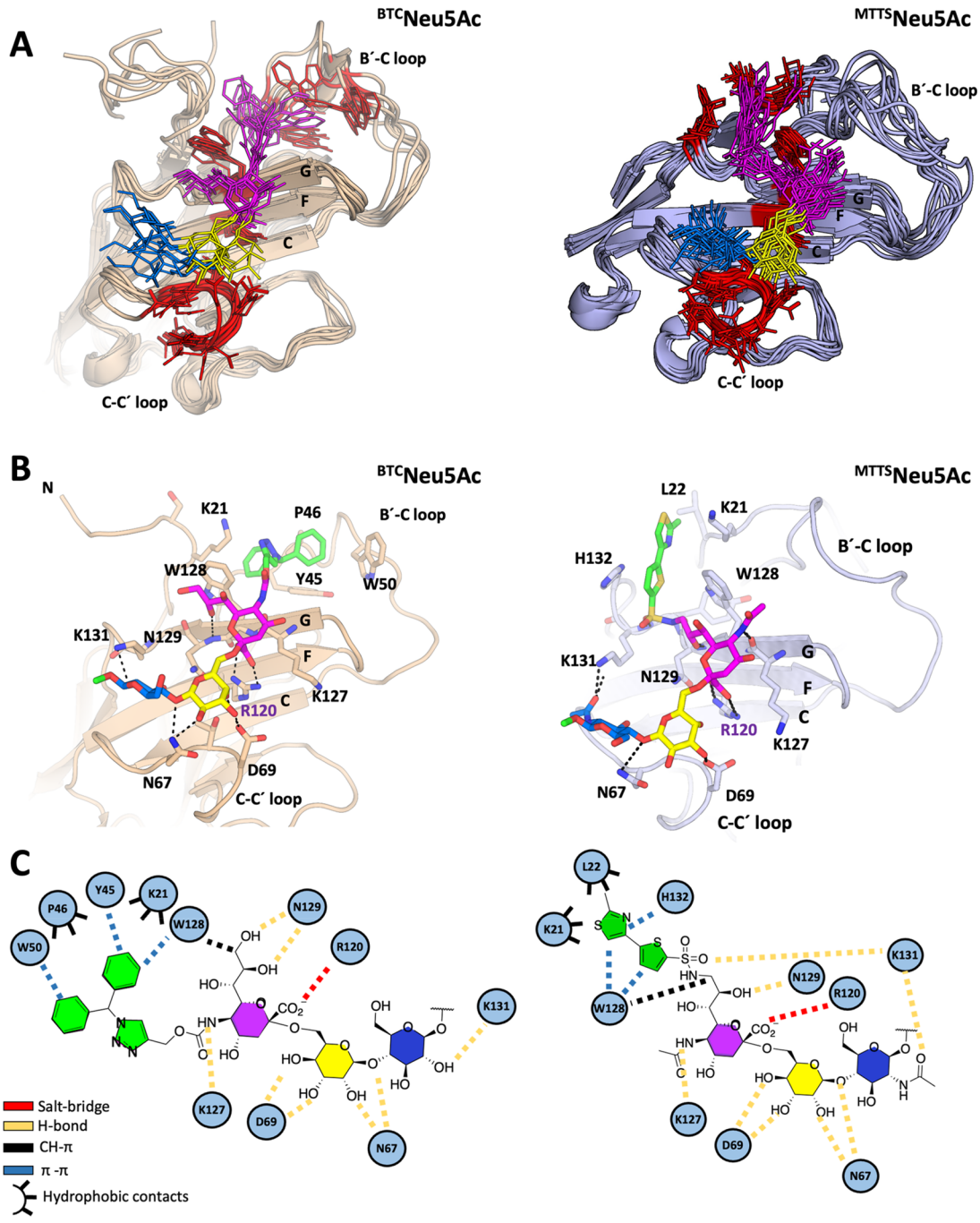

Figure 6. The 3D models of the complexes of ^{BTC}Neu5Ac and ^{MTTS}Neu5Ac with Siglec-9. (A) Superposition of the models from the MD calculations for the Siglec-9-^{BTC}Neu5Ac and with Siglec-9-^{MTTS}Neu5Ac complexes. (B) Representative 3D models of the Siglec-9 V-set Ig domain bound to ^{BTC}Neu5Ac and with ^{MTTS}Neu5Ac, as deduced from the MD simulation. (C) 2D interaction diagram highlighting the key intermolecular contacts responsible for the accommodation of ^{BTC}Neu5Ac (left) and ^{MTTS}Neu5Ac (right) in the Siglec-9 sialic-acid-binding domain. The computed intermolecular contacts and the geometries of the bound ligands are also depicted and are in full agreement with the ligand- and receptor-based NMR-based experimental observations.

were induced by ^{BTC}Neu5Ac at the N-terminus and the B′−C loops, strongly suggesting that these regions are involved in accommodating the 1-(diphenylmethyl)-1H-1,2,3-triazole moiety. Moreover, the exhaustive analysis of the CSP revealed that the side chains of W128Nε1-Hε1 (at the G strand) and W50Nε1-Hε1 (within the B′−C loop) showed their highest CSP in the presence of ^{BTC}Neu5Ac.

The analysis of the ^{1}H−^{15}N HSQC spectra for the interaction of Siglec-9 with ^{MTTS}Neu5Ac shows that the chemical exchange events are in the slow-intermediate regime on the NMR chemical shift time scale. In this case, the additional fragments are extended over position O9 at the glycerol chain of the sialic acid scaffold. Indeed, saturation of Siglec-9 was achieved after adding just eight ligand equivalents. Given the simultaneous existence of cross peaks for the apo and bound forms (Figure S9), integration of the corresponding peak volumes allowed estimating the binding affinity, with a remarkable K_D value of 13.9 ± 2.3 μM that is the same order of

https://doi.org/10.1021/acschembio.3c00664
ACS Chem. Biol. 2024, 19, 483−496

magnitude as the K_D determined by ITC (Figure 4). In contrast with the observations for the titration with ^{BTC}Neu5Ac, no meaningful perturbations were observed either for W50Nε1-Hε1 or for W50N-HN. Other residues at the B′−C loop presented only minor CSPs as well. However, Y130N-HN was severely shifted ($\Delta\delta$ 0.36 ppm in ^{1}H and 0.91 ppm in ^{15}N), while the W128Nε1-Hε1 peak vanished and did not recover (Figure S10). The presented evidence suggests that the binding mode of this aromatic scaffold differs from that displayed by the ^{BTC}Neu5Ac analogue.

Curiously, some of the duplicated cross peaks (*cis*−*trans* P53 isomerization) showed different CSP values in the presence of ^{BTC}Neu5Ac and ^{MTTS}Neu5Ac. In the case of ^{BTC}Neu5Ac, the analysis estimated a slightly better affinity for the Pro-*trans* versus the Pro-*cis* isomer (Figure S11). For instance, the K_D values estimated for some cross peaks in the *cis* form were 37 ± 5 μM (F43), 46 ± 9 μM (V66), and 37 ± 6 μM (G124). For the *trans* isomers, the K_D values were by a factor of 2 smaller: 23 ± 7 μM (F43), 23 ± 8 μM (V66), and 11 ± 5 μM (G124).

Three-Dimensional Models of Siglec-9 Bound to the Natural and Modified Glycans. Next, we combined the experimental data on the interaction of the glycans with Siglec-9 obtained through NMR with computational models and molecular dynamics (MD) simulations to gain additional insights into the recognition of sialoglycans by Siglec-9. In the absence of any 3D structure of Siglec-9, we employed RoseTTA fold[32] and AlphaFold[33,34] to model the V-set domain. These two sets of structures generated by the aforementioned software exhibited variations in the *cis*/*trans* conformation of the P53 residue within the B′−C loop (Figure S12). Considering the HNCO NMR data, where the most populated conformer observed was the *cis* conformation, we selected the model of AlphaFold for subsequent MD simulations. In the AphaFold model, a CH−π interaction between the aromatic ring of Y52 and the polarized Hα of P53 is established, which only takes place in the *cis*-Pro conformer (Figure S12B).

The starting geometries for the Siglec-9 and ^{BTC}Neu5Ac/^{MTTS}Neu5Ac complexes included initial positioning and relative orientation of the aromatic fragments guided by the observed bound-ligand conformations measured by NMR. The 3D model structures of the Siglec-9-ligand complexes were stable during the whole 500 ns simulation time, showing minor fluctuations around one well-defined geometry (Figure 6). Nevertheless, a certain flexibility was observed on the N-terminal and B′−C loop regions, as highlighted in Figure 6. The key intermolecular salt bridge interaction between the carboxylate (COO^-) group of the Neu5Ac moiety and the guanidinium of the R120 side chain was also kept (Figure 6). Moreover, in all cases, H9$_{proS}$ of the glycerol chain of the Neu5Ac residue established a CH-π sugar-aromatic stacking[35] with the indole ring of W128 (Figure 6 and Figures S13−S15), as also previously described for Siglec-7 and Siglec-8.[23,36] Hydroxyls O8 and OH9 interact via a hydrogen bond with the backbone amide and the carbonyl groups of N129, respectively. Additionally, H3 and H4 of the Neu5Ac make van der Waals contacts with the side chain of K127, while the *N*-acetyl group of the sialic acid provides a hydrogen bond with the backbone carbonyl of K127. The MD models satisfactorily account for the strong CSPs observed in the HSQC titrations for K127, W128, and N129, which likely arose as a consequence of the accommodation of the Neu5Ac monosaccharide fragment.

The obtained 3D models of Siglec9$_{d1}$with α2,3SLN, sLeX, and 6-*O*-sulfo-sLeX (Figure S14 and Figure S15) suggest that the N67, T68, and D69 residues at the C−C′ loop of the lectin are involved in the accommodation of the Fuc and Gal moieties. In the case of α2,3SLN, Gal establishes a H-bond interaction with the backbone amide of T68 and the carboxylate side chain of D69. In the case of sLeX and 6-*O*-sulfo sLeX ligands, the Fuc moiety contributes to the binding with additional H-bond interactions between Fuc and the side chains of N67 and D69. For the α2,3SLN case, T68 is heavily involved in the interaction, while the presence of the Fuc moiety in sLeX and 6-*O*-sulfo sLeX influences the N67 and D69 chemical shifts. According to the 3D model structure, the sulfate moiety in the 6-*O*-sulfo-sLeX glycan involves the G strand of the lectin, through the creation of an ion-pair interaction between the sulfate and the NH_3^+ group of K131 and a charge assisted H-bond with the amide side chain of N129. It is noteworthy in the MD simulations that the bound conformation of sLeX is very well-defined, as highlighted by the C−H···O hydrogen bond previously described.[28] In fact, the computed Φ/Ψ dihedral angles around the glycosidic linkages are in full agreement with the NOESY-derived distances, predicting a fairly stable bound conformation, with minor fluctuations around the global minimum, especially for the Galβ(1,4)Glc*N*Ac glycosidic linkage (Φ = 52 ± 8°, Ψ = 6 ± 6°). In contrast, for the α2,3SLN analogue, the same torsion angles display higher variations (Φ = 45 ± 23°, Ψ = −2 ± 19°), as shown in Figure S16, evidencing the conformational rigidification stabilized by the Fuc-Gal C−H···O hydrogen bond.

Interestingly, the glycan scaffold of ^{BTC}Neu5Ac and ^{MTTS}Neu5Ac showed common interactions with the N67, D69, R120, K127, W128, N129, and K131 of the C−C′ loop and the strands F and G during the MD simulation (Figure 5), also analogous to those computed for the α2,6SLN ligand. This match is also in agreement with the STD-NMR-based epitope map and observed CSPs. For ^{BTC}Neu5Ac, the 3D model can explain the observed CSPs for Nε1-Hε1 W128 and Nε1-Hε1 W50 (Figure 5 and Figure S13). In fact, there are stabilizing π−π stacking interactions between the corresponding indole rings of these two tryptophan side chains and the 1-(diphenylmethyl)-1H-1,2,3-triazole moiety of ^{BTC}Neu5Ac. Fittingly, the intramolecular NOEs observed between the aromatic protons and H9, H7, and H6 at the glycerol side chain of Neu5Ac can account for the spin-diffusion effect mediated by the indole ring of the W128 residue (Figure 5). The diphenylmethyl scaffold also interacts via π−π stacking with the Y45 side chain and also establishes hydrophobic contacts with the isomerizing P46 residue. This fact may explain the vanishment of the Y45 and S47 cross-peaks during the ^{1}H−^{15}N HSQC titration.

For ^{MTTS}Neu5Ac, the model suggests that W128, Y130, K131, and H132 within the G-strand are key for accommodating the 5-(2-methylthiazol-4-yl)thiophene-2-sulfonamide, along with K21 and L22 residues at the N-terminus. Indeed, the large deshielding observed for the amide proton of Y130 is in full agreement with the intermolecular hydrogen bond between this amide moiety and the sulfonamide group of ^{MTTS}Neu5Ac (Figure S13). Moreover, in the 3D model, the MTTS fragment establishes π−π stacking interactions with the W128 and H133 aromatic side chains and protrudes into the

https://doi.org/10.1021/acschembio.3c00664
ACS Chem. Biol. 2024, 19, 483−496

hydrophobic pocket. This orientation also accounts for the large perturbation observed in the W128Nε1-Hε1 cross peak during the titration. Inside the hydrophobic pocket, the thiazole stabilizes hydrophobic contacts with the aliphatic side chains of K21 and L22 residues. These interactions nicely explain the disappearance of the L22 and L23 cross peaks during the titration. Additionally, for ^{MTTS}Neu5Ac, with the aromatic substituent at position C9, the experimental distance of 2.7 Å between H4 of the thiophene and H5 of the thiazole moieties could be deduced in the bound state from the trNOE analysis. The MD simulation points out that these heteroaromatic rings are positioned coplanar with their hydrogen atoms pointing outward. Furthermore, additional trNOEs were observed between the H3 of the thiophene and the $H9_{proS}$, $H9_{proR}$, and H8 of Neu5Ac, suggesting a particular presentation of the heteroaromatic ring toward the sialic acid scaffold.

DISCUSSION

Siglec-9 is an inhibitory glycoimmune checkpoint receptor of particular interest in the context of tumor immunotherapy, as it is believed to suppress antitumor immune responses through engagement to sialoglycans expressed on cancer cells, suggesting that this axis constitutes an interesting target for checkpoint inhibition.[4,5,37] Conversely, the use of Siglec ligand analogs with improved affinities have been exploited to recruit Siglecs to enhance suppression of unwanted immune responses.[5−7] As demonstrated by different glycan array experiments, Siglec-9 exhibits broad specificity for natural sialic acid ligands, with a slight preference for those presenting sialyl Lewis X (sLeX) and its 6-O sulfo analogue as terminal epitopes.[38,39] Notably, sLeX-containing glycans are prominently expressed as terminal epitopes on mucin *O*-glycans, including the well-studied tumor-associated MUC1, which has been recognized as a Siglec-9 binder.[2,40] However, it is crucial to highlight that there is a lack of observed binding effects of Siglec-9 toward the *O*-glycoengineered cell libraries and *O*-glycodomain reporters, including MUC1.[41,42] Moreover, the impact of Siglec-9 binding on fucosylated cellular ligands, known to influence Siglec interactions,[43] has not been addressed. This notable gap in our understanding underscores the need for further investigations into the specificity and binding dynamics of Siglec-9 with diverse glycan structures, including fucosylated ligands and *O*-glycoengineered libraries.

In order to generate modified sialic-acid-based ligands with higher affinity, it has been found that Siglecs bind in general preferably to analogues with relatively bulky and hydrophobic substituents at C5 and C9, but not both.[17] Furthermore, there appears to be little preference for the underlying glycosidic linkage between Neu5Ac and the next monosaccharide, suggesting that the binding occurs mostly through the modified sialic acid moiety. A detailed molecular information on the interactions between Siglec-9 and sialoglycans will help explain the preferences of this receptor for naturally expressed ligands (e.g., sLeX or 6-*O*-sulfo sLeX) and will boost the development of synthetic sialoglycans.

Here, the molecular recognition features and preferences of Siglec-9 toward the naturally expressed α2,6SLN, α2,3SLN, sLeX, and 6-*O*-sulfo-sLeX have been revealed using a combination of NMR spectroscopy and MD simulations. The preference of Siglec-9 for the 6-*O*-sulfo sLeX glycan is evident. The Fuc moiety is located close to the C−C′ loop, while the sulfate interacts with the side chains of the N129 and K131 residues which protrude from the G strand toward the inside of the binding groove. Additionally, the Fuc moiety conformationally constrains the sLeX tetrasaccharide into its bioactive conformation, minimizing the entropic penalty of the binding, and thus making it a better binder.[44] In Siglec-9, the α2,6SLN scaffold caused less CSP than the α2,3SLN glycan, meaning the preference of this Siglec toward α2,3 glycosidic linkage between the terminal Neu5Ac and the underlying Gal.

In the quest toward generating specific and high-affinity modified sialoglycans for targeting Siglec-9, the synthetic analogues ^{MTTS}Neu5Ac and ^{BTC}Neu5Ac were identified from a synthetic glycan library.[8] The K_D values as determined herein from the CSPs and ITC demonstrate that, while ^{MTTS}Neu5Ac and ^{BTC}Neu5Ac are elaborated with the less preferred α2,6 glycosidic linkage, they exhibit higher affinity toward Siglec-9 as a result of their respective substituents.[2] Thus, the substituents at C5 and C9 at Neu5Ac, respectively, are the main driving forces of the observed improved binding toward Siglec-9. Indeed, an enthalpy−entropy compensation phenomenon describes the binding of ^{BTC}Neu5Ac and ^{MTTS}Neu5Ac to Siglec-9, with a better binding enthalpy observed for the ^{MTTS}Neu5Ac. As demonstrated by MD, consistent with the obtained NMR data, more stabilizing intermolecular $\pi-\pi$ stacking and H-bond contacts with Siglec-9 were found to be present with the 5-(2-methylthiazol-4-yl)thiophene side chain and the sulfonamide group of the ^{MTTS}Neu5Ac ligand, thus explaining the observed enthalpy differences. The ^{MTTS}Neu5Ac scaffold displays more torsional degrees of freedom between the additional molecular fragments and the sugar core, which may also explain the observed higher entropic penalty.

We also suggest that the rigidification of the lateral chains of ^{BTC}Neu5Ac provides the key interactions with Siglec-9, which could lead to a lesser entropy penalty in comparison with ^{MTTS}Neu5Ac. The MD simulations further suggest that the heteroaromatic rings of MTTS bind in a coplanar orientation, with their hydrogen atoms pointing outward, in agreement with the NOE-based experimental distance in the bound state between H4 of the thiophene and H5 of the thiazole moieties (2.7 Å). Furthermore, additional trNOEs were observed between the H3 of the thiophene and $H9_{proS}$, $H9_{proR}$, and H8 of Neu5Ac, suggesting a particular and well-defined presentation of the heteroaromatic ring toward the sialic. Nevertheless, it may also be possible that the larger hydrophobic surface of the 1-(diphenylmethyl)-1H-1,2,3-triazole unit might replace more water molecules from the hydrophobic binding pocket of Siglec-9 in comparison to the heteroaromatic scaffold of ^{MTTS}Neu5Ac. Alternatively, both rigidification and solvation/desolvation events can contribute to the observed distinct entropy penalty for both glycomimetics.

Despite the high amino acid sequence similarity between Siglec-7 and Siglec-9, major differences have been described in their preferences for glycan binding. Previous studies have reported that Siglec-7 selectively binds to α(2,8)-disialylated sialosides,[45,46] while Siglec-9 shows a preference for 6-*O*-sulfo-sLeX.[39] However, recent findings have challenged the notion that Siglec-7 recognizes gangliosides with 2,8-linked sialic acids. Instead, it has been postulated that it selectively binds to disialylated *O*-glycan tetrasaccharides found on mucin-type glycoproteins, such as CD43.[47]

Our structural and molecular recognition analysis of Siglec-9 shows that ligand selectivity, in comparison with Siglec-7, is mainly due to key structural differences in the C−C′ and B−C′

https://doi.org/10.1021/acschembio.3c00664
ACS Chem. Biol. 2024, 19, 483−496

loops (Figure S13). The extended C−C′ loop of Siglec-7 drives the preference of this lectin toward longer ligands, such as α(2,8)-disialylated sialosides (G1Tb),[23] compared to Siglec-9. However, Siglec-9 possesses a longer and more flexible B−C′ loop comprised by three extra aromatic amino acids, which make the accommodation of modified sialosides with aromatic moieties at Neu5Ac C5 suitable (Figure S13).

The experimental observations by Nycholat et al.[15] pointed out that MTT-bearing sialosides also bind Siglec-8. Structural comparison between Siglec-8 (PDB ID 7QUI) and Siglec-9, reveals that the hydrophobic residues present at the uniquely large G-G′ loop of Siglec-8 may interact with the MTTS scaffold (Figure S13). In contrast, ^{BTC}Neu5Ac is recognized by Siglec-9 by accommodating the 1-(diphenylmethyl)-1H-1,2,3-triazole scaffold in the highly flexible B′−C loop. This B′−C loop in Siglec-9 is longer and more flexible than those in Siglec-7 and Siglec-8 (Figure S13). Moreover, it harbors the two aromatic residues Y45 and W50. Therefore, relative to the natural ligands ^{BTC}Neu5Ac exhibits both higher specificity and higher affinity with K_D values in the medium-low micromolar range, as deduced by ITC and NMR, for Siglec-9. The combination of decorations at C5 and C9 could lead to an improved glycan mimetic possessing both high-affinity and specificity for Siglec-9, as modeled in Figure S17. Further studies on this direction are currently underway.

Overall, our experimental data unveil for the first time the molecular details of the interaction of the human immune checkpoint receptor Siglec-9 with its preferred natural sialoglycan ligands (sLeX and 6-O sulfo sLeX) and explain how chemical modifications with aromatic substituents at the C5 and C9 positions of Neu5Ac can enhance the binding affinity far beyond those of natural ligands in this specific case. Due to the presence of the unique B′−C loop in Siglec-9, we infer that modifications at the C5 of Neu5Ac bear the greatest potential for establishing specificity toward Siglec-9.

MATERIALS AND METHODS

Detailed procedures for molecular cloning, protein expression and purification, NMR protein backbone assignment, and isothermal titration calorimetry experiments can be found in the Supporting Information.

NMR Binding Studies. The total volume for the NMR samples was 500 μL, and 5 mm precision NMR tubes were used (New Era Enterprises, Vineland, USA). The pH of the samples was monitored with a Crison Basic 20 pH meter (Crison Instruments SA, Barcelona, Spain) and adjusted if necessary with NaOH or HCl. All of the saturation transfer difference (STD NMR) experiments were recorded in a Bruker AVANCE 2 600 MHz spectrometer equipped with a standard triple-channel probe and in a Bruker 800 MHz Bruker spectrometer with a cryoprobe (Bruker, Billerica, MA, United States).

The NMR samples were prepared in deuterated saline-phosphate buffer (sodium phosphate, 20 mM; NaCl, 150 mM; pH 7.4). The standard ligand/Siglec-9 ratio was 1:40 for all of the molecules where the protein (unlabeled) concentration was kept at 50 μM in all cases. STD experiments were recorded at 298 K. For all of the STD and trNOESY experiments, Siglec-$9_{d1\text{-}d3}$-mVenus produced in HEK293F cells were used, in order to diminish the appearance of potential protein signals in the spectra due to its higher molecular weight (65 kDa), which provides a fast T_2 relaxation rate and a faster transmission of STD and trNOESY informations.

An in-house 1D STD sequence using 12.5 ms PC9 pulses was used. A T2 filter of 100 ns was employed with the aim of reducing the protein signals. For the natural ligands α2,3SLN, α2,6SLN, and sLeX, 2 s of saturation time was used. However, for the ^{BTC}Neu5Ac and ^{MTTS}Neu5Ac glycomimetics, STD NMR spectra at different saturation times (0.5 1, 2, and 4 s) were recorded in order to plot a build-up curve and to normalize the acquired saturation of protons at different functional groups. The following monoexponential function was applied:

$$\begin{aligned} \mathrm{STD}(t_{sat}) &= \mathrm{STD}^{max}\cdot(1 - e^{-k_{sat}t_{sat}}) \\ \frac{d(\mathrm{STD}(t_{sat}))}{d(t_{sat})} &= \mathrm{STD}^{max}\cdot k_{sat}\cdot e^{-k_{sat}t_{sat}} \xrightarrow{t_{sat}=0} \frac{d(\mathrm{STD}(t_{sat}))}{d(t_{sat})} \\ &= \mathrm{STD}^{max}\cdot k_{sat} \end{aligned}$$

where $\mathrm{STD}(t_{sat})$ stands for the observed STD intensity at a given saturation time (t), STD^{max} is the maximal obtainable STD signal when a long saturation time is applied, and k_{sat} indicates the observable saturation rate constant. After the fitting, multiplication of STD^{max} and k_{sat} gave the slope of the curve when the saturation time went to zero.

All of the STD experiments were recorded with a relaxation delay (d1) of 5 s. The off-resonance frequency was set at −30 ppm and the on-resonance frequency at 0.77 ppm for all of the experiments except for glycan mimetic ^{MTTS}Neu5Ac, where it was irradiated at −0.03 ppm due to the proximity of ligand signals. Blank STD-NMR spectra for the protein in the absence of ligands were also acquired, irradiating at both 0.77 and −0.03 ppm.

For the NOESY experiments, all the samples were prepared in deuterated phosphate-buffered saline (20 mM sodium phosphate, 150 mM NaCl, pH 7.4). A protein concentration of 50 μM was used with a protein/ligand ratio of 1:10 for the ligands α2,3SLN, α2,6SLN, sLeX, ^{BTC}Neu5Ac, and ^{MTTS}Neu5Ac. All experiments were acquired at 298 K. An in-house NOESY sequence was used for all of the experiments. NOESY experiments for the free form of the ligands were acquired at a 400 ms mixing time. However, in the presence of Siglec-$9_{d1\text{-}d3}$-mVenus, these experiments were recorded using 100 and 200 ms mixing times, in order to avoid the presence of spin-diffusion effects.

The ^{1}H−^{15}N HSQC experiments were acquired by using a Bruker AVANCE 2 800 MHz spectrometer equipped with cryoprobe. The samples were prepared by using sodium phosphate 20 mM, NaCl 150 mM, at a pH of 7.4, made up with a mix of 90% H_2O/10% D_2O. For all of the measurements, 50 μM of uniformly ^{15}N-labeled Siglec-9_{d1} was used except for ligand 6-*O*-sulfo sLeX where the protein concentration was set to 126 μM. Different equivalents of ligands (stocks at 100 mM concentration) were added until complete or almost complete saturation of Siglec-9 was reached. The experiments were carried out at 293 K. In all of the cases, 32 scans were acquired with 192 (t1) × 1536 (t2) complex data points in ^{15}N and ^{1}H dimensions, respectively. For analyzing the obtained data, CcpNmr Analysis software was employed. Average chemical shift changes were calculated by using the following equation:

$$\delta_{average} = \sqrt{\frac{1}{2}[\Delta\delta_H^2 + (0.14\Delta\delta_N)^2]}$$

For determining the K_D of the ligands, CcpNmr Analysis was used, where the following nonlinear least-squares fit for the employed amino acids was used:

$$\Delta\delta_{obs} = \Delta\delta_{\infty}\left(\frac{([P] + [L] + K_d) - \sqrt{([L] + [P] + K_d)^2 - 4[P][L]}}{2[P]}\right)$$

For the titration of the ^{MTTS}Neu5Ac that was in the slow exchange regime, K_D was calculated by integrating the NMR peaks corresponding to the protein apo [P] and bound [PL] states at 0.8 equiv (40 μM) of the total ligand ([L]t = [L] + [PL]). The total protein concentration ([P]t = [P] + [PL]) is 50 μM. Since the [P]/[PL] value can be measured in the HSQC spectrum from the integrals for the free and bound protein species, the K_D value can be easily estimated by developing and solving the canonical mass action law equation:

https://doi.org/10.1021/acschembio.3c00664
ACS Chem. Biol. 2024, 19, 483−496

$$K_D = \frac{[P][L]}{[PL]}$$

Molecular Dynamics (MD) Simulations. The homology model of the V-Ig domain of Siglec-9 was constructed using RoseTTAFold[32] and AlphaFold.[33] An AlphaFold-built homology model (P53 in *cis*) was used to run MD simulations with all of the ligands (Figure S18). A model built with RoseTTAFold (P53 in *trans*) was used to run an MD simulation just with ^{BTC}Neu5Ac (Figure S18), in order to compare the difference in the binding mode of this glycomimetic when Siglec-9 is found in *cis* and in *trans* configurations.

The glycans were manually docked within the sialic acid binding site by superimposing the Siglec-9 homology model with the cocrystallized X-ray structure of Siglec-8 with ^{NSA}Neu5Ac (PDB ID: 7QUI). The corresponding ligand was superposed to the cocrystallized ^{NSA}Neu5Ac, adopting the same geometry as the Neu5Ac of the glycomimetic. The docked glycans within the Siglec-9 presented the bioactive conformation deduced from the trNOESY NMR. The lateral chain of the ^{BTC}Neu5Ac was placed within the B′−C loop and N-terminal chain, close to residues K21, L22, Y45, and W50, since it was observed by ^{1}H−^{15}N HSQC that these residues were the most perturbed ones in this case. Regarding the ^{MTTS}Neu5Ac, the lateral chain conformation was determined by trNOESY NMR, and this was fitted within the hydrophobic cleft formed between W128 and H132, as indicated by ^{1}H−^{15}N HSQC NMR.

Then, MD simulations were carried out with the AMBER 20[48] package implemented with *ff14SB*[49] for the protein. For the natural glycans α2,3SLN, α2,6SLN, sLeX, and 6-*O*-sulfo sLeX, the GLYCAM06j-1[50] force field was used, while for the glycan mimetics ^{BTC}Neu5Ac and ^{MTTS}Neu5Ac the general Amber force field (GAFF2)[51] force field was chosen. For building the molecules, the initial structures were neutralized with either Na^+ or Cl^- ions and set at the center of a cubic TIP3P[52] water box with a buffering distance between the solute and a box of 10 Å. For each system, we followed a two-stage geometry optimization approach: the first stage minimizes only the positions of solvent molecules and ions, and the second stage is an unrestrained minimization of all of the atoms in the simulation cell. The systems were then heated by increasing the temperature from 0 to 300 K under a constant pressure of 1 atm and periodic boundary conditions. Harmonic restraints of 10 kcal mol^{-1} were applied to the solute, under the Andersen temperature coupling scheme.[53] The time step was kept at 1 fs during the heating stages, allowing potential inhomogeneities to self-adjust. Water molecules were treated with the SHAKE[54] algorithm such that the angle between the hydrogen atoms is kept fixed through the simulations. Long-range electrostatic effects were modeled using the particle mesh Ewald (PME) method.[55] An 8 Å cutoff was applied to nonbonded interactions. Each system was equilibrated for 2 ns with a 2 fs time step at a constant volume and temperature of 300 K. Five independent production trajectories were then run for an additional 500 ns under the same simulation conditions, leading to accumulated simulation times of 2.5 μs for each system.

■ ASSOCIATED CONTENT

Supporting Information

The Supporting Information is available free of charge at https://pubs.acs.org/doi/10.1021/acschembio.3c00664.

Detailed materials and methods, including the source of ligands; cloning, expression, and purification of Siglec-9; NMR backbone assignment; and isothermal titration calorimetry; supporting tables, figures, and references (PDF)

■ AUTHOR INFORMATION

Corresponding Authors

Jesús Jiménez-Barbero − *Chemical Glycobiology Lab, Center for Cooperative Research in Biosciences (CIC bioGUNE), Basque Research and Technology Alliance (BRTA), 48160 Derio, Bizkaia, Spain; Ikerbasque, Basque Foundation for Science, 48009 Bilbao, Biscay, Spain; Department of Organic and Inorganic Chemistry, Faculty of Science and Technology, University of the Basque Country, EHU-UPV, 48940 Leioa, Bizkaia, Spain; Centro de Investigacion Biomedica en Red de Enfermedades Respiratorias, 28029 Madrid, Spain;* orcid.org/0000-0001-5421-8513; Email: jjbarbero@cicbiogune.es

June Ereño-Orbea − *Chemical Glycobiology Lab, Center for Cooperative Research in Biosciences (CIC bioGUNE), Basque Research and Technology Alliance (BRTA), 48160 Derio, Bizkaia, Spain; Ikerbasque, Basque Foundation for Science, 48009 Bilbao, Biscay, Spain;* orcid.org/0000-0002-5076-2105; Email: jereno@cicbiogune.es

Authors

Unai Atxabal − *Chemical Glycobiology Lab, Center for Cooperative Research in Biosciences (CIC bioGUNE), Basque Research and Technology Alliance (BRTA), 48160 Derio, Bizkaia, Spain;* orcid.org/0000-0002-0546-8521

Corwin Nycholat − *Departments of Molecular Medicine and Immunology and Microbiology, The Scripps Research Institute, La Jolla, California 92037, United States*

Johannes M. Pröpster − *Institute of Molecular Biology and Biophysics, ETH Zurich, 8093 Zurich, Switzerland*

Andrea Fernández − *Chemical Glycobiology Lab, Center for Cooperative Research in Biosciences (CIC bioGUNE), Basque Research and Technology Alliance (BRTA), 48160 Derio, Bizkaia, Spain*

Iker Oyenarte − *Chemical Glycobiology Lab, Center for Cooperative Research in Biosciences (CIC bioGUNE), Basque Research and Technology Alliance (BRTA), 48160 Derio, Bizkaia, Spain*

Maria Pia Lenza − *Chemical Glycobiology Lab, Center for Cooperative Research in Biosciences (CIC bioGUNE), Basque Research and Technology Alliance (BRTA), 48160 Derio, Bizkaia, Spain*

Antonio Franconetti − *Chemical Glycobiology Lab, Center for Cooperative Research in Biosciences (CIC bioGUNE), Basque Research and Technology Alliance (BRTA), 48160 Derio, Bizkaia, Spain;* orcid.org/0000-0002-7972-8795

Cátia O. Soares − *Associate Laboratory i4HB - Institute for Health and Bioeconomy, NOVA School of Science and Technology and UCIBIO, Department of Chemistry, Faculdade de Ciências e Tecnologia, Universidade NOVA de Lisboa, 2829-516 Caparica, Portugal*

Helena Coelho − *Associate Laboratory i4HB - Institute for Health and Bioeconomy, NOVA School of Science and Technology and UCIBIO, Department of Chemistry, Faculdade de Ciências e Tecnologia, Universidade NOVA de Lisboa, 2829-516 Caparica, Portugal;* orcid.org/0000-0003-1992-8557

Filipa Marcelo − *Associate Laboratory i4HB - Institute for Health and Bioeconomy, NOVA School of Science and Technology and UCIBIO, Department of Chemistry, Faculdade de Ciências e Tecnologia, Universidade NOVA de Lisboa, 2829-516 Caparica, Portugal*

Mario Schubert − *Institute of Molecular Biology and Biophysics, ETH Zurich, 8093 Zurich, Switzerland; Department of Biosciences and Molecular Biology, University of Salzburg, 5020 Salzburg, Austria;* orcid.org/0000-0003-0278-4091

https://doi.org/10.1021/acschembio.3c00664
ACS Chem. Biol. 2024, 19, 483−496

James C. Paulson − *Departments of Molecular Medicine and Immunology and Microbiology, The Scripps Research Institute, La Jolla, California 92037, United States;* orcid.org/0000-0003-4589-5322

Complete contact information is available at: https://pubs.acs.org/10.1021/acschembio.3c00664

Author Contributions

Experimental conception and design: J.E.-O., J.J-B.; data acquisition: U.A., M.P.L., H.C., C.S., I.O., A. F., M.S., C.N., J.E.-O.; analysis of data: U.A., M.P.L., H.C., A. F., M.S., J.J.-B., J.E.-O., J.P.; drafting the article or revising it critically for important intellectual content: U.A., M.S., F.M., J.C.P., J.E.-O., J.J.-B.

Notes

The authors declare no competing financial interest.

■ ACKNOWLEDGMENTS

This work was supported by the European Research Council (788143-RECGLYCANMR to J.J.-B.) and the Marie-Skłodowska-Curie actions (ITN Glytunes grant agreement no. 956758 to J.E.-O. and ITN BactiVax under grant agreement no. 860325 to J.J.-B. & U.A.). F.M., C.S., and H.C. acknowledge Fundação para a Ciência e a Tecnologia (FCT-Portugal) for funding projects PTDC/BIA-MIB/31028/2017 and UCIBIO project (UIDP/04378/2020 and UIDB/04378/2020) and Associate Laboratory Institute for Health and Bioeconomy i4HB project (LA/P/0140/2020) and to the CEEC contracts 2020.00233.CEECIND and 2020.03261.CEECIND for F.M. and H.C., respectively. The NMR spectrometers at Lisbon are part of the National NMR Network (PTNMR) and are partially supported by Infrastructure Project No. 22161 (cofinanced by FEDER through COMPETE 2020, POCI and PORL and FCT through PIDDAC). The Bilbao lab acknowledge the NMR resources and the technical support provided by the Euskadi NMR lab (LRE) of the ICTS "Red de Laboratorios de RMN de biomoléculas (R-LRB)" of Spain.F.M. and J.J.B. acknowledge to the European commission for the COST Action 18132 GLYCONANOPROBES. We thank Agencia Estatal de Investigación of Spain for grants PID2019-107770RA-I00 (J.E.-O.) and the Severo Ochoa Center of Excellence Accreditation CEX2021-001136-S, all funded by MCIN/AEI/10.13039/501100011033. We also thank CIBERES, an initiative of Instituto de Salud Carlos III (ISCIII, Madrid, Spain).

■ REFERENCES

(1) Zhang, J. Q.; Nicoll, G.; Jones, C.; Crocker, P. R. Siglec-9, a Novel Sialic Acid Binding Member of the Immunoglobulin Superfamily Expressed Broadly on Human Blood Leukocytes. *J. Biol. Chem.* **2000**, *275* (29), 22121−22126.

(2) Beatson, R.; Tajadura-Ortega, V.; Achkova, D.; Picco, G.; Tsourouktsoglou, T.-D.; Klausing, S.; Hillier, M.; Maher, J.; Noll, T.; Crocker, P. R.; Taylor-Papadimitriou, J.; Burchell, J. M. The Mucin MUC1 Modulates the Tumor Immunological Microenvironment through Engagement of the Lectin Siglec-9. *Nat. Immunol* **2016**, *17* (11), 1273−1281.

(3) Avril, T.; Floyd, H.; Lopez, F.; Vivier, E.; Crocker, P. R. The Membrane-Proximal Immunoreceptor Tyrosine-Based Inhibitory Motif Is Critical for the Inhibitory Signaling Mediated by Siglecs-7 and −9, CD33-Related Siglecs Expressed on Human Monocytes and NK Cells. *J. Immunol.* **2004**, *173* (11), 6841−6849.

(4) González, G.; Lakatos, K.; Hoballah, J.; Fritz-Klaus, R.; Al-Johani, L.; Brooker, J.; Jeong, S.; Evans, C. L.; Krauledat, P.; Cramer, D. W.; Hoffman, R. A.; Hansen, W. P.; Patankar, M. S. Characterization of Cell-Bound CA125 on Immune Cell Subtypes of Ovarian Cancer Patients Using a Novel Imaging Platform. *Cancers (Basel)* **2021**, *13* (9), 2072.

(5) Ibarlucea-Benitez, I.; Weitzenfeld, P.; Smith, P.; Ravetch, J. V. Siglecs-7/9 Function as Inhibitory Immune Checkpoints in Vivo and Can Be Targeted to Enhance Therapeutic Antitumor Immunity. *Proc. Natl. Acad. Sci. U. S. A.* **2021**, *118* (26), No. e2107424118.

(6) Rodriguez, E.; Boelaars, K.; Brown, K.; Eveline Li, R. J.; Kruijssen, L.; Bruijns, S. C. M.; van Ee, T.; Schetters, S. T. T.; Crommentuijn, M. H. W.; van der Horst, J. C.; van Grieken, N. C. T.; van Vliet, S. J.; Kazemier, G.; Giovannetti, E.; Garcia-Vallejo, J. J.; van Kooyk, Y. Sialic Acids in Pancreatic Cancer Cells Drive Tumour-Associated Macrophage Differentiation via the Siglec Receptors Siglec-7 and Siglec-9. *Nat. Commun.* **2021**, *12* (1), 1270.

(7) Läubli, H.; Nalle, S. C.; Maslyar, D. Targeting the Siglec−Sialic Acid Immune Axis in Cancer: Current and Future Approaches. *Cancer Immunol Res.* **2022**, *10* (12), 1423−1432.

(8) Stanczak, M. A.; Siddiqui, S. S.; Trefny, M. P.; Thommen, D. S.; Boligan, K. F.; von Gunten, S.; Tzankov, A.; Tietze, L.; Lardinois, D.; Heinzelmann-Schwarz, V.; von Bergwelt-Baildon, M.; Zhang, W.; Lenz, H.-J.; Han, Y.; Amos, C. I.; Syedbasha, M.; Egli, A.; Stenner, F.; Speiser, D. E.; Varki, A.; Zippelius, A.; Läubli, H. Self-Associated Molecular Patterns Mediate Cancer Immune Evasion by Engaging Siglecs on T Cells. *J. Clin. Invest.* **2018**, *128* (11), 4912−4923.

(9) Belisle, J. A.; Horibata, S.; Jennifer, G. A.; Petrie, S.; Kapur, A.; André, S.; Gabius, H.-J.; Rancourt, C.; Connor, J.; Paulson, J. C.; Patankar, M. S. Identification of Siglec-9 as the Receptor for MUC16 on Human NK Cells, B Cells, and Monocytes. *Mol. Cancer* **2010**, *9* (1), 118.

(10) Wu, Y.; Huang, W.; Xie, Y.; Wang, C.; Luo, N.; Chen, Y.; Wang, L.; Cheng, Z.; Gao, Z.; Liu, S. Siglec-9, a Putative Immune Checkpoint Marker for Cancer Progression Across Multiple Cancer Types. *Front Mol. Biosci* **2022**, *9*, No. 743515.

(11) Wang, J. H. S.; Jiang, N.; Jain, A.; Lim, J. Development of Effective Siglec-9 Antibodies Against Cancer. *Curr. Oncol Rep* **2023**, *25* (1), 41−49.

(12) Yokoi, H.; Choi, O. H.; Hubbard, W.; Lee, H.-S.; Canning, B. J.; Lee, H. H.; Ryu, S.-D.; von Gunten, S.; Bickel, C. A.; Hudson, S. A.; MacGlashan, D. W.; Bochner, B. S. Inhibition of FcεRI-Dependent Mediator Release and Calcium Flux from Human Mast Cells by Sialic Acid−Binding Immunoglobulin-like Lectin 8 Engagement. *Journal of Allergy and Clinical Immunology* **2008**, *121* (2), 499−505.e1.

(13) Lenza, M. P.; Atxabal, U.; Oyenarte, I.; Jiménez-Barbero, J.; Ereño-Orbea, J. Current Status on Therapeutic Molecules Targeting Siglec Receptors. *Cells* **2020**, *9* (12), 2691.

(14) Chen, W. C.; Completo, G. C.; Sigal, D. S.; Crocker, P. R.; Saven, A.; Paulson, J. C. In Vivo Targeting of B-Cell Lymphoma with Glycan Ligands of CD22. *Blood* **2010**, *115* (23), 4778−4786.

(15) Nycholat, C. M.; Duan, S.; Knuplez, E.; Worth, C.; Elich, M.; Yao, A.; O'Sullivan, J.; McBride, R.; Wei, Y.; Fernandes, S. M.; Zhu, Z.; Schnaar, R. L.; Bochner, B. S.; Paulson, J. C. A Sulfonamide Sialoside Analogue for Targeting Siglec-8 and-F on Immune Cells. *J. Am. Chem. Soc.* **2019**, *141* (36), 14032−14037.

(16) Duan, S.; Arlian, B. M.; Nycholat, C. M.; Wei, Y.; Tateno, H.; Smith, S. A.; Macauley, M. S.; Zhu, Z.; Bochner, B. S.; Paulson, J. C. Nanoparticles Displaying Allergen and Siglec-8 Ligands Suppress IgE-FcεRI−Mediated Anaphylaxis and Desensitize Mast Cells to Subsequent Antigen Challenge. *J. Immunol.* **2021**, *206* (10), 2290−2300.

(17) Rillahan, C. D.; Schwartz, E.; McBride, R.; Fokin, V. V.; Paulson, J. C. Click and Pick: Identification of Sialoside Analogues for Siglec-Based Cell Targeting. *Angew. Chem.* **2012**, *124* (44), 11176−11180.

(18) Delaveris, C. S.; Wilk, A. J.; Riley, N. M.; Stark, J. C.; Yang, S. S.; Rogers, A. J.; Ranganath, T.; Nadeau, K. C.; Blish, C. A.; Bertozzi,

C. R. Synthetic Siglec-9 Agonists Inhibit Neutrophil Activation Associated with COVID-19. *ACS Cent. Sci.* **2021**, *7*, 650−657.
(19) Delaveris, C. S.; Chiu, S. H.; Riley, N. M.; Bertozzi, C. R. Modulation of Immune Cell Reactivity with Cis-Binding Siglec Agonists. *Proc. Natl. Acad. Sci. U. S. A.* **2021**, *118* (3), 1−11.
(20) Angata, T.; Varki, A. Cloning, Characterization, and Phylogenetic Analysis of Siglec-9, a New Member of the CD33-Related Group of Siglecs: Evidence for Co-Evolution with Sialic Acid Synthesis Pathways. *J. Biol. Chem.* **2000**, *275* (29), 22127−22135.
(21) Movsisyan, L. D.; Macauley, M. S. Structural Advances of Siglecs: Insight into Synthetic Glycan Ligands for Immunomodulation. *Org. Biomol Chem.* **2020**, *18* (30), 5784−5797.
(22) Blixt, O.; Collins, B. E.; van den Nieuwenhof, I. M.; Crocker, P. R.; Paulson, J. C. Sialoside Specificity of the Siglec Family Assessed Using Novel Multivalent Probes. *J. Biol. Chem.* **2003**, *278* (33), 31007−31019.
(23) Attrill, H.; Imamura, A.; Sharma, R. S.; Kiso, M.; Crocker, P. R.; Van Aalten, D. M. F. Siglec-7 Undergoes a Major Conformational Change When Complexed with the α(2,8)-Disialylganglioside GT1b. *J. Biol. Chem.* **2006**, *281* (43), 32774−32783.
(24) Pröpster, J. M.; Yang, F.; Ernst, B.; Allain, F. H. T.; Schubert, M. Functional Siglec Lectin Domains from Soluble Expression in the Cytoplasm of Escherichia Coli. *Protein Expr Purif* **2015**, *109*, 14−22.
(25) Schubert, M.; Labudde, D.; Oschkinat, H.; Schmieder, P. A Software Tool for the Prediction of Xaa-Pro Peptide Bond Conformations in Proteins Based on 13 C Chemical Shift Statistics. *J. Biomol. NMR* **2002**, *24*, 149.
(26) Zaccai, N. R.; Maenaka, K.; Maenaka, T.; Crocker, P. R.; Brossmer, R.; Kelm, S.; Jones, E. Y. Structure-Guided Design of Sialic Acid-Based Siglec Inhibitors and Crystallographic Analysis in Complex with Sialoadhesin. *Structure* **2003**, *11* (5), 557−567.
(27) Poppe, L.; Stuike-Prill, R.; Meyer, B.; van Halbeek, H. The Solution Conformation of Sialyl-α(2→6)-Lactose Studied by Modern NMR Techniques and Monte Carlo Simulations. *J. Biomol NMR* **1992**, *2* (2), 109−136.
(28) Aeschbacher, T.; Zierke, M.; Smieško, M.; Collot, M.; Mallet, J.-M.; Ernst, B.; Allain, F. H.-T.; Schubert, M. A Secondary Structural Element in a Wide Range of Fucosylated Glycoepitopes. *Chem.—Eur. J.* **2017**, *23* (48), 11598−11610.
(29) Peccati, F.; Jiménez-Osés, G. Enthalpy−Entropy Compensation in Biomolecular Recognition: A Computational Perspective. *ACS Omega* **2021**, *6* (17), 11122−11130.
(30) Crocker, P. R.; Paulson, J. C.; Varki, A. Siglecs and Their Roles in the Immune System. *Nat. Rev. Immunol* **2007**, *7* (4), 255−266.
(31) Angata, T.; Hingorani, R.; Varki, N. M.; Varki, A. Cloning and Characterization of a Novel Mouse Siglec, MSiglec-F: Differential Evolution of the Mouse and Human (CD33) Siglec-3-Related Gene Clusters. *J. Biol. Chem.* **2001**, *276* (48), 45128−45136.
(32) Baek, M.; DiMaio, F.; Anishchenko, I.; Dauparas, J.; Ovchinnikov, S.; Lee, G. R.; Wang, J.; Cong, Q.; Kinch, L. N.; Schaeffer, R. D.; Millan, C.; Park, H.; Adams, C.; Glassman, C. R.; DeGiovanni, A.; Pereira, J. H.; Rodrigues, A. V.; van Dijk, A. A.; Ebrecht, A. C.; Opperman, D. J.; Sagmeister, T.; Buhlheller, C.; Pavkov-Keller, T.; Rathinaswamy, M. K.; Dalwadi, U.; Yip, C. K.; Burke, J. E.; Garcia, K. C.; Grishin, N. V.; Adams, P. D.; Read, R. J.; Baker, D. Accurate Prediction of Protein Structures and Interactions Using a Three-Track Neural Network. *Science (1979)* **2021**, *373* (6557), 871−876.
(33) Jumper, J.; Evans, R.; Pritzel, A.; Green, T.; Figurnov, M.; Ronneberger, O.; Tunyasuvunakool, K.; Bates, R.; Žídek, A.; Potapenko, A.; Bridgland, A.; Meyer, C.; Kohl, S. A. A.; Ballard, A. J.; Cowie, A.; Romera-Paredes, B.; Nikolov, S.; Jain, R.; Adler, J.; Back, T.; Petersen, S.; Reiman, D.; Clancy, E.; Zielinski, M.; Steinegger, M.; Pacholska, M.; Berghammer, T.; Bodenstein, S.; Silver, D.; Vinyals, O.; Senior, A. W.; Kavukcuoglu, K.; Kohli, P.; Hassabis, D. Highly Accurate Protein Structure Prediction with AlphaFold. *Nature* **2021**, *596* (7873), 583−589.
(34) Mirdita, M.; Schütze, K.; Moriwaki, Y.; Heo, L.; Ovchinnikov, S.; Steinegger, M. ColabFold: Making Protein Folding Accessible to All. *Nature Methods 2022 19:6* **2022**, *19* (6), 679−682.
(35) Asensio, J. L.; Ardá, A.; Cañada, F. J.; Jiménez-Barbero, J. Carbohydrate−Aromatic Interactions. *Acc. Chem. Res.* **2013**, *46* (4), 946−954.
(36) Lenza, M. P.; Atxabal, U.; Nycholat, C.; Oyenarte, I.; Franconetti, A.; Quintana, J. I.; Delgado, S.; Núñez-Franco, R.; Garnica Marroquín, C. T.; Coelho, H.; Unione, L.; Jiménez-Oses, G.; Marcelo, F.; Schubert, M.; Paulson, J. C.; Jiménez-Barbero, J.; Ereño-Orbea, J. Structures of the Inhibitory Receptor Siglec-8 in Complex with a High-Affinity Sialoside Analogue and a Therapeutic Antibody. *JACS Au* **2023**, *3* (1), 204−215.
(37) Haas, Q.; Boligan, K. F.; Jandus, C.; Schneider, C.; Simillion, C.; Stanczak, M. A.; Haubitz, M.; Seyed Jafari, S. M.; Zippelius, A.; Baerlocher, G. M.; Laubli, H.; Hunger, R. E.; Romero, P.; Simon, H.-U.; von Gunten, S. Siglec-9 Regulates an Effector Memory $CD8^+$ T-Cell Subset That Congregates in the Melanoma Tumor Microenvironment. *Cancer Immunol Res.* **2019**, *7* (5), 707−718.
(38) Bull, C.; Nason, R.; Sun, L.; Van Coillie, J.; Madriz Sørensen, D.; Moons, S. J.; Yang, Z.; Arbitman, S.; Fernandes, S. M.; Furukawa, S.; McBride, R.; Nycholat, C. M.; Adema, G. J.; Paulson, J. C.; Schnaar, R. L.; Boltje, T. J.; Clausen, H.; Narimatsu, Y. Probing the Binding Specificities of Human Siglecs by Cell-Based Glycan Arrays. *Proc. Natl. Acad. Sci. U. S. A.* **2021**, *118* (17), No. e2026102118.
(39) Yu, H.; Gonzalez-Gil, A.; Wei, Y.; Fernandes, S. M.; Porell, R. N.; Vajn, K.; Paulson, J. C.; Nycholat, C. M.; Schnaar, R. L. Siglec-8 and Siglec-9 Binding Specificities and Endogenous Airway Ligand Distributions and Properties. *Glycobiology* **2017**, *27* (7), 657−668.
(40) Beatson, R.; Graham, R.; Grundland Freile, F.; Cozzetto, D.; Kannambath, S.; Pfeifer, E.; Woodman, N.; Owen, J.; Nuamah, R.; Mandel, U.; Pinder, S.; Gillett, C.; Noll, T.; Bouybayoune, I.; Taylor-Papadimitriou, J.; Burchell, J. M. Cancer-Associated Hypersialylated MUC1 Drives the Differentiation of Human Monocytes into Macrophages with a Pathogenic Phenotype. *Commun. Biol.* **2020**, *3* (1), 644.
(41) Gao, C.; Hanes, M. S.; Byrd-Leotis, L. A.; Wei, M.; Jia, N.; Kardish, R. J.; McKitrick, T. R.; Steinhauer, D. A.; Cummings, R. D. Unique Binding Specificities of Proteins toward Isomeric Asparagine-Linked Glycans. *Cell Chem. Biol.* **2019**, *26* (4), 535−547.e4.
(42) Narimatsu, Y.; Joshi, H. J.; Nason, R.; Van Coillie, J.; Karlsson, R.; Sun, L.; Ye, Z.; Chen, Y.-H.; Schjoldager, K. T.; Steentoft, C.; Furukawa, S.; Bensing, B. A.; Sullam, P. M.; Thompson, A. J.; Paulson, J. C.; Büll, C.; Adema, G. J.; Mandel, U.; Hansen, L.; Bennett, E. P.; Varki, A.; Vakhrushev, S. Y.; Yang, Z.; Clausen, H. An Atlas of Human Glycosylation Pathways Enables Display of the Human Glycome by Gene Engineered Cells. *Mol. Cell* **2019**, *75* (2), 394−407.e5.
(43) Brinkman-Van der Linden, E. C. M.; Varki, A. New Aspects of Siglec Binding Specificities, Including the Significance of Fucosylation and of the Sialyl-Tn Epitope. *J. Biol. Chem.* **2000**, *275* (12), 8625−8632.
(44) Zierke, M.; Smieško, M.; Rabbani, S.; Aeschbacher, T.; Cutting, B.; Allain, F. H.-T.; Schubert, M.; Ernst, B. Stabilization of Branched Oligosaccharides: Lewis ^{x} Benefits from a Nonconventional C−H···O Hydrogen Bond. *J. Am. Chem. Soc.* **2013**, *135* (36), 13464−13472.
(45) Nicoll, G.; Avril, T.; Lock, K.; Furukawa, K.; Bovin, N.; Crocker, P. R. Ganglioside GD3 Expression on Target Cells Can Modulate NK Cell Cytotoxicity via Siglec-7-dependent and -independent Mechanisms. *Eur. J. Immunol.* **2003**, *33* (6), 1642−1648.
(46) Hashimoto, N.; Ito, S.; Tsuchida, A.; Bhuiyan, R. H.; Okajima, T.; Yamamoto, A.; Furukawa, K.; Ohmi, Y.; Furukawa, K. The Ceramide Moiety of Disialoganglioside (GD3) Is Essential for GD3 Recognition by the Sialic Acid−Binding Lectin SIGLEC7 on the Cell Surface. *J. Biol. Chem.* **2019**, *294* (28), 10833−10845.
(47) Wisnovsky, S.; Möckl, L.; Malaker, S. A.; Pedram, K.; Hess, G. T.; Riley, N. M.; Gray, M. A.; Smith, B. A. H.; Bassik, M. C.; Moerner, W. E.; Bertozzi, C. R. Genome-Wide CRISPR Screens Reveal a Specific Ligand for the Glycan-Binding Immune Checkpoint Receptor

https://doi.org/10.1021/acschembio.3c00664
ACS Chem. Biol. 2024, 19, 483−496

Siglec-7. *Proc. Natl. Acad. Sci. U. S. A.* **2021**, *118* (5), No. e2015024118.
(48) Case, D. A.; Belfon, K.; Ben-Shalom, I. Y.; Brozell, S. R.; Cerutti, D. S.; Cheatham, T. E., III; Cruzeiro, V. W. D.; Darden, T. A.; Duke, R. E.; Giambasu, G.; Gilson, M. K.; Gohlke, H.; Goetz, A. W.; Harris, R.; Izadi, S.; Izmailov, S. A.; Kasavajhala, K.; Kovalenko, A.; Krasny, R.; York, D. M.; Kollman, P. A. *AMBER 2020*; University of California: San Francisco, 2020.
(49) Maier, J. A.; Martinez, C.; Kasavajhala, K.; Wickstrom, L.; Hauser, K. E.; Simmerling, C. Ff14SB: Improving the Accuracy of Protein Side Chain and Backbone Parameters from Ff99SB. *J. Chem. Theory Comput* **2015**, *11* (8), 3696−3713.
(50) Kirschner, K. N.; Yongye, A. B.; Tschampel, S. M.; González-Outeiriño, J.; Daniels, C. R.; Foley, B. L.; Woods, R. J. GLYCAM06: A Generalizable Biomolecular Force Field. Carbohydrates. *J. Comput. Chem.* **2008**, *29* (4), 622−655.
(51) Wang, J.; Wolf, R. M.; Caldwell, J. W.; Kollman, P. A.; Case, D. A. Development and Testing of a General Amber Force Field. *J. Comput. Chem.* **2004**, *25* (9), 1157−1174.
(52) Jorgensen, W. L.; Chandrasekhar, J.; Madura, J. D.; Impey, R. W.; Klein, M. L. Comparison of Simple Potential Functions for Simulating Liquid Water. *J. Chem. Phys.* **1983**, *79* (2), 926−935.
(53) Andersen, H. C. Molecular Dynamics Simulations at Constant Pressure and/or Temperature. *J. Chem. Phys.* **1980**, *72* (4), 2384−2393.
(54) Miyamoto, S.; Kollman, P. A. Settle: An Analytical Version of the SHAKE and RATTLE Algorithm for Rigid Water Models. *J. Comput. Chem.* **1992**, *13* (8), 952−962.
(55) Darden, T.; York, D.; Pedersen, L. Particle Mesh Ewald: An N·log(N) Method for Ewald Sums in Large Systems. *J. Chem. Phys.* **1993**, *98* (12), 10089−10092.
(56) Kim, D. E.; Chivian, D.; Baker, D. Protein Structure Prediction and Analysis Using the Robetta Server. *Nucleic Acids Res.* **2004**, *32*, W526−W531.

https://doi.org/10.1021/acschembio.3c00664
ACS Chem. Biol. 2024, 19, 483−496